Ball Screw Health Monitoring with Inertial Sensors

Vibhor Pandhare, Marcella Miller, Gregory William Vogl, and Jay Lee

***Abstract*—In industrial applications, the mechanical wear on ball screw components can lead to a loss of positioning accuracy that reduces the operational reliability and reproducibility of production systems. Existing monitoring solutions are impractical for real industrial settings or are unable to provide quantifiable estimates of the magnitude of degradation. To address this, the proposed method strategically applies a two-phase data collection with inertial sensors to perform both health monitoring and fault magnitude estimation. The first, online phase offers a practical, non-intrusive means of monitoring the ball screw degradation during normal production operations. As deemed necessary by the first phase, the second, offline phase is implemented outside the production routine to physically quantify the detected fault. The combined methods offer a balanced approach that provides detailed information while still considering the requirements of a production environment. To validate the performance of this proposed strategy, a run-to-failure experiment was performed on a linear axis testbed. Validation results indicate that the method is a pragmatic and promising approach for incipient fault detection and absolute backlash error measurement in a linear axis.**

***Index Terms*—Backlash Estimation, Ball Screw, Correlation Analysis, Health Monitoring, Inertial Measurement Unit**

I. Introduction

A ball screw, used within a linear positioning system, is a complex, high-precision component used to convert rotary motion into linear motion. Ball screws have wide industry applications, especially as feed drive systems in computer numerical controlled (CNC) machines and industrial robots. In many high-precision manufacturing systems, the functioning of a ball screw can profoundly affect the operation accuracy and reproducibility of the entire system. Up to 19% of machine tool failures can be related to degradation of the ball screw [1, 2]. In semiconductor manufacturing processes, imprecision in a robotic arm operation due to a degraded ball screw can cause expensive damage to wafer products. Therefore, it is critical to develop a system that can detect the ball screw degradation at an early stage and predict its future degradation trajectory with actionable intelligence.

The linear positioning system, also known as a linear axis, could have multiple failure modes [3]. Mechanically, the entire system undergoes cyclic loading as the loaded carriage is moved back and forth. One of the most common but critical failure modes is the loss of rigidity of the system due to usage, also known as preload loss, occurring mainly between the ball screw and the ball nut [4-8]. When assembling a linear axis system, oversized balls are typically used in the ball nut and the trucks to eliminate internal clearances and increase rigidity and motion precision. This act creates an initial preload between the ball screw and the ball nut or between the trucks and the rails. However, mechanical wear will typically cause the oversized balls to progressively become small enough that preload is lost, causing mechanical backlash and resulting in a reversal error at a position [9]. Such changes in the linear axis can eventually lead to the loss of positioning accuracy, resulting in non-conforming behavior.

Multiple methods have been developed to monitor preload loss and backlash. However, the methods either need offline data collection, require extensive geometrical parameters of the linear axis that may be difficult to procure in industrial applications, or cannot estimate the magnitude of backlash, which is important to evaluate the performance accuracy against the acceptable tolerances to ensure operation quality.

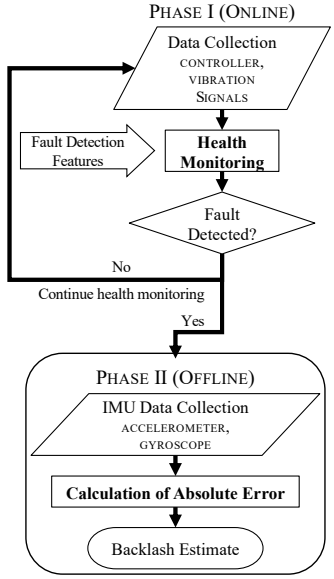

Fig. 1. Overview of the proposed two-phase methodology for practical monitoring of ball screws.

Manuscript received January 23, 2022; revised June 13, 2022 and August 5, 2022; accepted September 13, 2022. Paper no. TII-22-0373. (Corresponding author: Vibhor Pandhare)

Vibhor Pandhare, Marcella Miller and Jay Lee are with the Department of Mechanical and Materials Engineering, College of Engineering and Applied Sciences, University of Cincinnati, 560 Baldwin Hall, Cincinnati, OH, USA 45221 (e-mail: pandhavr@mail.uc.edu; mille5mc@mail.uc.edu; jay.lee@uc.edu)

Gregory William Vogl is with the Engineering Laboratory, National Institute of Standards and Technology, 100 Bureau Drive, Gaithersburg, MD, USA 20899-8220 (e-mail: gregory.vogl@nist.gov)

Furthermore, offline instrumentation or cutting tests that estimate backlash are often utilized too late, after ball screw errors have already impacted the production of components.

Thus, a practical two-phase approach, as presented in Fig. 1, is proposed to monitor ball screw health using inertial sensors and forms the core novelty of the work. The first phase is a method for fault detection in the ball screw using vibration sensors and controller signals. This phase of the methodology is used to monitor ball screws from the beginning of use until an incipient fault is detected. Once a fault is detected, the second phase of the methodology is used to quantify the fault by estimating the absolute backlash error using an inertial measurement unit (IMU). The estimation of the backlash directly tracks the impact of the fault on the operation, allowing the user to schedule maintenance or replacement as needed. The proposed methodology is validated on an experimental test bed in which a linear axis is run until a backlash failure mode is reached.

The remainder of the article is organized as follows. Section II presents the literature review. Section III describes the experimental test bed and data acquisition procedure. Sections IV and V describe the Phase I and Phase II methods and discuss corresponding results for the experiment. Section VI concludes the article.

II. Literature Review

In a linear positioning system, preload loss results in gradual degradation of performance and can lead to excessive vibration and the loss of operation accuracy in the form of backlash or reversal error [6]. Since this fault mode compromises the carefully selected initial rigidity of the system which enables precise, repeatable motion to occur, close monitoring of the degradation trend has been an increasingly popular topic in the literature.

Tsai, et al. [5] proposed a method to determine the onset of preload loss in a ball screw feed drive system by monitoring the change of ball pass frequency. Other studies also suggest monitoring shifts in the frequency spectrum to estimate preload loss or backlash. [7, 10] use vibration, position, and current information to quantify the continuous relationship between axial natural frequency and preload for real-time reporting. Xi, et al. [11] estimate both the preload loss and backlash increase by tracking the shift in the resonance frequency. Feng and Pan [12] exploits the relationship between peak rotational frequency and changes in the preload, and Benker, et al. [13] investigate the influence of preload level on the behavior of the transfer function. While these methods show promising relationships between the degradation and the frequency spectrum, some of the research endeavors do not investigate the development of preload loss over long-term operation. Moreover, they only detect the onset of preload loss while neglecting to quantify the extent of degradation and to track the loss severity that can be leveraged for prognostics.

Developing dynamic, physics-based models is also a common approach for monitoring. The work in Ref. [7, 10] relies on a complex model representation of ball screw dynamics to implement preload tracking. Wang, et al. [14] use a preload degradation model to explore the effects of feed rate, external load, and machining errors on the rate of preload loss**.** In Ref. [15], the Hertz contact theory and Archard wear model are used to build load distribution and velocity variation models to predict the preload values. Although these approaches typically produce accurate results, the use of such dynamic equations requires prior knowledge of the ball screw's mechanical parameters, such as various stiffness coefficients and Young's modulus, and geometric properties [7]. In practice, these parameters are difficult to determine beforehand and may vary over different systems due to manufacturing and assembly variations and errors.

Outside of these popular categories, many other approaches have been documented. The method proposed by Feng and Pan [16] uses support vector machine (SVM) learning to classify the severity of preload degradation based on vibration and temperature data. Huang, et al. [17] similarly use an SVM on features extracted from vibration, current, speed, and encoder signals. Denkena, et al. [18] investigated the capability of sensor fusion based on principal component analysis to monitor preload loss of single nut ball screws. Pandhare, et al. [19] studied cross-sensor domain adaptation for diagnosing discrete variations in preload level and backlash. More experiments have traced preload loss through the measure of frictional torque [20] or through a finite element method-based procedure [21, 22]. Benker and Zaeh [23] employ a convolutional neural network (CNN) to identify different fault conditions and preload levels. These methods are useful for analyzing the preload level and backlash, but often attempt to treat the degradation as a discrete rather than continuous condition; the issue is framed as a classification rather than a health monitoring problem.

Expanding the investigation to encompass other intelligent machine learning methods, deep learning is often applied for the health monitoring of industrial assets, and many improvements have been made to boost model performance. The maximum mean discrepancy metric is embedded in a CNN, and cross-domain classification for discrete ball screw health conditions is performed by Azamfar, et al. [24]. Li, et al. [25] also investigated the cross-domain performance of deep neural networks and proposes that class-level domain adaptation be used in conjunction with domain-level adaptation for improved results. Shao, et al. [26] use a modified CNN to perform fault diagnosis under the assumption of limited training data. Zhao, et al. [27] and Zhao, et al. [28] sought to improve the generalization capabilities of the trained model by introducing additional constraints and loss functions into the network. Similarly, Zhao, et al. [29] add an adaptive focal loss function to their variational auto-encoder to address the problem of an imbalanced class distribution condition in the training data, and Zhao, et al. [30] focus on achieving fault diagnosis with only limited labeled data. While all the proposed methods outperform other state of the art algorithms for the fault diagnosis tasks, the deep learning solutions require proper hyperparameter selections in order to produce good results, and hyperparameter optimization can be difficult to achieve. These advancements in the deep learning-based methods offer extremely high accuracy for fault diagnosis tasks, but they are less used for prognosis.

Rather, to quantify the fault severity, direct methods of fault measurement were established [31]. However, these are typically manual, time-consuming processes that interrupt

production and increase machine downtime. Manufacturers need automated and efficient procedures to estimate the degradation with minimal disruptions to production. Towards this end, the hybrid data- and physics-driven models in Refs. [32] and [33] successfully employ a particle filter-based approach to estimate the system backlash and use the resulting values for further remaining useful life prediction. Considering data-driven approaches, Vogl, et al. [34] developed a method to use data from an IMU for identification of changes in the translational and angular errors due to axis degradation. While the developed method was evaluated for estimation of wear on the rails of the ball screw guideways [35], backlash remains largely unaddressed by the purely data-driven methods.

Therefore, to overcome the identified gaps in the literature and motivated by the challenges of preload loss and backlash tracking, this paper presents a practical two-phase approach to monitor ball screw health using inertial sensors and offers the following contributions:

1) A preselected set of features for monitoring the continuous preload loss degradation trend via PCA-T^2 is provided. It is proposed that the features can be used to assess the health of new systems.

2) New data-driven methods for quantifying the system backlash using IMU data are described. These methods require minimal knowledge of nominal ball screw parameters.

3) The proposed methods are combined to provide a practical, non-intrusive approach to linear axis monitoring that can be deployed in a real industrial setting. These methods are then applied to an experimental run-to-failure dataset.

III. Experimental Test Bed and Data Acquisition Setup

Fig. 2 shows the linear axis experimental testbed used for this study. The linear axis was screwed on top of a concrete slab weighing approximately 1700 kg (3800 lbs.). A ball screw rotates via a motor to move the carriage nominally parallel with the X-axis. Four trucks with ball bearings contact two rails to constrain the carriage to move in a nominally linear manner along the guideway for a total possible travel of 450 mm. The carriage will run back and forth continuously for months to undergo degradation, and to speed up this process, the carriage is loaded with steel weights totaling 100 kg (220 lbs.). Two triaxial accelerometers with a nominal sensitivity of 100 mV/g are attached to the ball nut, and an IMU, composed of a triaxial accelerometer and a triaxial rate gyroscope, is attached on top of the steel weights. The analog accelerometer in the IMU has a bandwidth from 0 Hz to 300 Hz (corresponding to the half-power point), a nominal sensitivity of 2000 mV/g, and a noise output of 7 μg rms/√Hz, while the digital rate gyroscope in the IMU has a half-power bandwidth from 0 Hz to 200 Hz and a noise output of 35 (μrad/s)/√Hz. In addition to controller data, data from these twelve inertial sensors is captured during axis degradation.

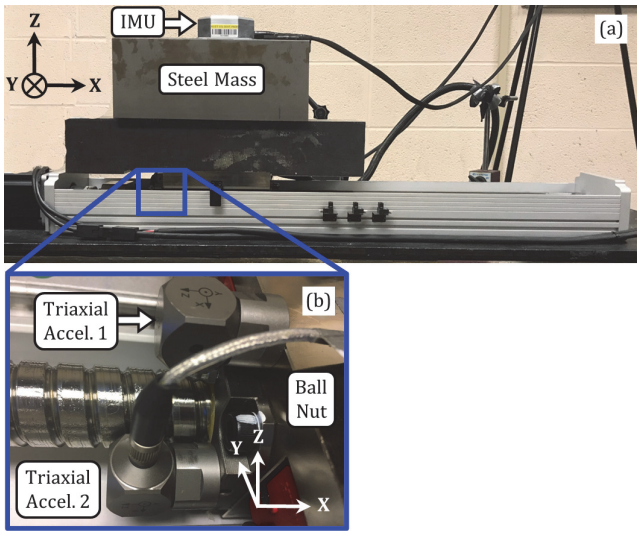

Fig. 2. (a) Linear axis with an IMU on the steel mass and (b) detail of sensor location of two triaxial accelerometers on the ball nut.

The new linear axis was run to failure (RTF) with a data collection strategy resembling real-life operation and monitoring. As proposed, data collection for monitoring ball screw health was performed in two phases. The details of the Phase I and Phase II data collection procedures are explained below in detail in Section A and Section B, respectively. A summary of the information in these two sections is shown in TABLE I.

TABLE I
Data Acquisition Summary

	Phase I (RTF Data)	Phase II (IMU Data)
speed(s)	400 mm/s	20, 100, 500 mm/s
acceleration	4,087.44 mm/s^2	19,600 mm/s^2
x_{start}	110 mm	0 mm
x_{end}	330 mm	450 mm
dwell time	1 s	10 s
acquisition method	24/7 (except during IMU runs)	90 runs twice a week
acquisition frequency	10 s every 30 min.	continuous

A. Phase-I Data Collection Routine

The linear axis was moved back and forth continuously, day and night, with a centered 220-mm-long stroke (movement between 110 mm and 330 mm relative to the zero position), which is about half of the total possible travel. The axis moves in a positive and negative direction at 400 mm/s. There was a one second pause after each direction of movement. This continuous movement represented the regular operation of a linear axis in industry. Data collection begins after an initial warmup operation period of nominally 2 h to avoid undesirable transient behavior. In this first phase, 10 s of data was collected every 30 minutes with a sampling rate of 10 kHz. This collection mode represents data collection for online incipient fault detection. Eight signals were collected in total: controller speed, controller torque, and X-axis, Y-axis, and Z-axis outputs from the two triaxial accelerometers on the ball nut.

B. Phase-II Data Collection Routine

Every three or four days, the first phase is temporarily interrupted by the second phase of data collection. In this second phase, the axis is moved back and forth with a full stroke of 450 mm. Each run consists of the axis moving back and forth at a slow speed (20 mm/s), then at a moderate speed

(100 mm/s), and then at a fast speed (500 mm/s). Ninety runs are performed in this second phase. Due in part to the 10s dwell time in between each of these motions, data collection occurs over a period of 3 h. IMU data is acquired for each run at a sampling rate of about 1613 Hz for the triaxial accelerometer and a sampling rate of about 1000 Hz for the triaxial rate gyroscope. This represents the offline monitoring procedure for estimating the magnitude of backlash in the ball screw motion. It is important to note that, for industrial applications, Phase II is proposed to be performed after a fault has been detected using the Phase I method, but for validation purposes, Phase II is performed right from the beginning of the experiments.

C. Overall Data Collection Routine

This two-phase experimental data collection was repeated until the ball screw reached an ultimate failure point of greater than 10 µm, per manufacturer guidance. Throughout the experiment, no lubrication was applied to the ball screw. A timeline of key events that occurred during the experiment is shown in TABLE II. The experiment was active for days 0 through 38, 116 through 255, and 377 through 574. During this time, the ball screw accumulated 8693 operation hours. For days 38 through 116 and days 255 through 377, the experiment was paused due to extenuating circumstances. These pauses did generate minimal short-term thermal effects on the data immediately after the experiment was resumed. To account for a fully cooled system, the nominal 2h system warmup time for Phase I data collection was adjusted; however, since the proposed method is developed to track the long-term, irreversible effects of physical damage, these thermal influences did not have any effect on the overall results.

TABLE II
EXPERIMENT TIMELINE

Day	Ball Screw Operation Hours	Event
0	0	start
38	855.5	pause
116	855.5	resume
255	4033	pause
377	4033	resume
574	8693	end

Periodically when switching from the first to the second phase, an additional step is taken to acquire backlash measurements that track the degradation of the axis over time. A dial indicator with a gradation of 12.7 µm is used, and sub-gradation measurements were estimated by eye. The lever of the dial indicator is set to rotate in the XY plane and is positioned so that its tip is almost touching the steel weights on the ball screw carriage. Once the dial indicator is in position, it is fixed via a magnetic base to the testbed base. The ball screw is then commanded to move successive fixed distances with an interval of 1 µm while dial indications are measured, from which the position of first contact by the lever of the dial indicator is determined by human inspection. This procedure is then repeated multiple times in both positive and negative directions, except that for the negative direction, the position of last contact is determined. The difference of the two positions (the first contact for the positive-direction motion, and the last contact for the negative-direction motion) for the repeated measurements is used to obtain an average reversal error or backlash value.

IV. PHASE I - ONLINE INCIPIENT FAULT DETECTION AND FAULT MAGNITUDE TRACKING

Vibration spectrum analysis and motor torque information are used to detect deviations from the healthy behavior of the ball screw under fixed operating conditions. A round of data collection in Phase I consists of multiple instances of the eight signals collected in a 10 s interval as described in the previous section. For each round, ten instances are selected, and each undergoes data preprocessing and segmentation, as presented in Fig. 3, to extract signal profiles at specific moments from the continuous back-and-forth motion. The speed signal is used as the reference to extract a steady-state segment of the accelerometer and torque signals as well as a transient segment of the torque signal. For every steady-state segment in a sample, a Hanning window is applied and the power spectral density (PSD) is calculated. Finally, the PSDs of all ten segments are averaged to create one representative PSD for each of the data collection rounds. Sample torque and accelerometer PSD values at t_a = 858.5 h and t_b = 8693 h of operation are shown in Fig. 4. The figure also shows three frequencies of interest (dotted lines) as well as the amplitudes of each PSD corresponding to the rotational frequency of 40 Hz (dashed lines). X1(X2), Y1(Y2), and Z1(Z2) are the X-, Y-, and Z-axis accelerations for the first(second) triaxial accelerometer on the ball nut.

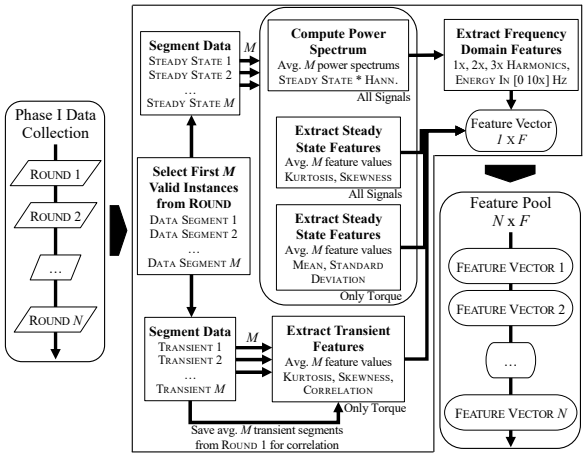

Fig. 3. An overview of Signal Preprocessing and Feature Extraction for Monitoring Methodology Phase I.

From the PSD of each of the seven signals, three features are extracted: the amplitudes of the PSD at the rotational frequency and the first two harmonics (80 Hz and 120 Hz). The energy of each PSD between 0 Hz and the 10th harmonic (400 Hz) is calculated for the six accelerometer signals. Time domain features (skewness and kurtosis) are extracted from the ten instances for steady-state segments of all accelerometer signals, and for both steady-state and transient segments of the torque signal. The ten resulting values for each feature type are averaged to generate the final feature values for the sample. Similarly, from the transient segments for the torque signal

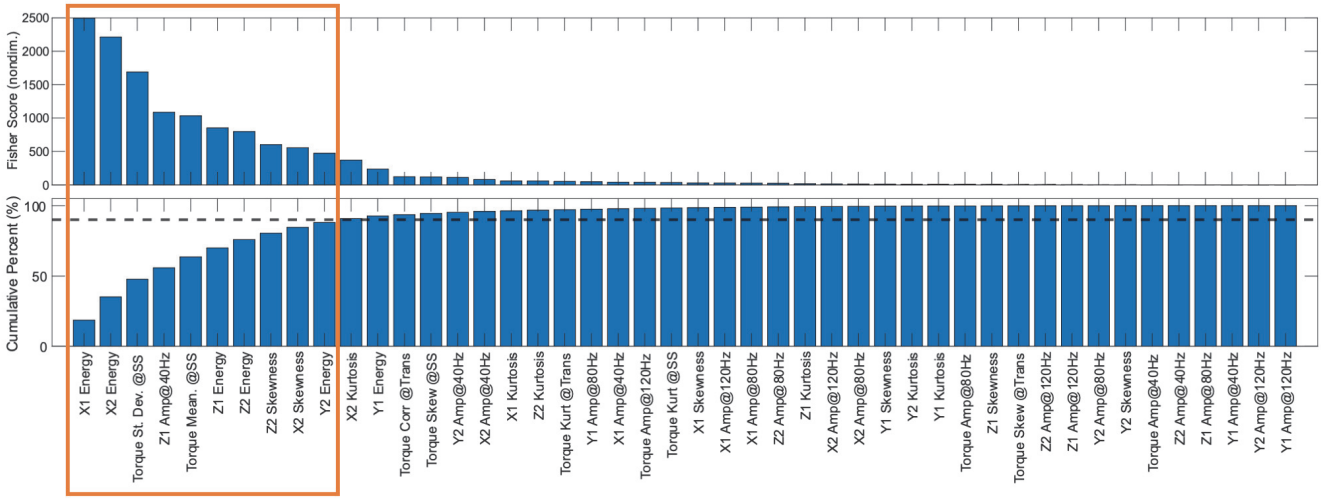

Fig. 5. Feature Selection using Fisher Scores and Cumulative Summation of Fisher Scores with 90% Threshold.

only, the correlation with the average transient torque segment from the first round of data collection is extracted. In total, 46 features are extracted and normalized to a mean of zero and a standard deviation of one.

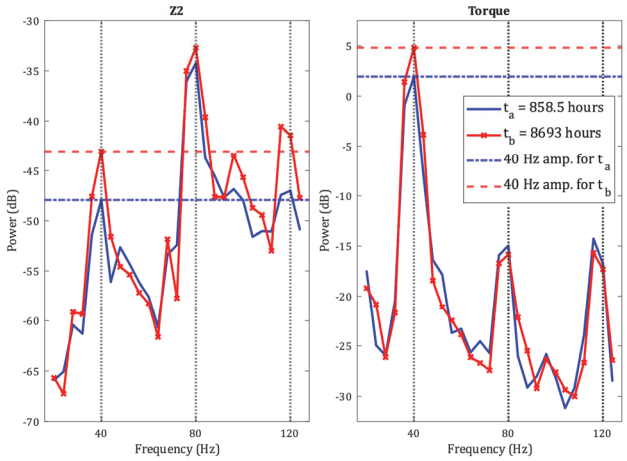

Fig. 4. Example PSD for the ball screw near the beginning and end of the RTF experiment.

To select appropriate features for fault detection out of the extracted 46 features, the Fisher criteria [36] is used. A reference experimental dataset [6] with known discrete ball screw conditions, including a backlash fault, is used to learn useful features for fault detection. The same process is followed for this dataset to extract the same set of 46 features. Features corresponding to the healthy samples and faulty samples with backlash error are assigned binary labels of healthy and faulty, respectively. The Fisher score for each feature is then calculated as

$$FisherScore = \frac{(\mu_H - \mu_F)^2}{\sigma_H^2 + \sigma_F^2} \quad (1)$$

where μ_H and μ_F indicate the mean of the feature for the healthy and faulty samples, respectively, while σ_H^2 and σ_F^2 indicate variances for the same [36]. Fig. 5 shows the Fisher scores and their corresponding normalized cumulative sum. A threshold of 90% of the cumulative sum is used to select the features for fault detection. It can be observed that the highlighted ten features constitute 90% of the total discriminating power of the total feature set and are thus selected.

Principal component analysis with Hotelling's T^2 statistic (PCA-T^2) [37, 38] is used to detect signs of an incipient fault in the system. The first fifteen samples (corresponding to approximately the first 1250 h of ball screw operation) are then used as baseline data while the remaining samples are used for testing. The principal components (PCs) of the normalized fault detection feature matrix were calculated. The number of principal components corresponding to at least 95% of the variance of the original features were retained. The statistical limit is calculated using

$$T_\alpha^2 = \frac{r(N-1)}{N-r} F_{r,N-r,\alpha} \quad (2)$$

where N is the number of samples in the training dataset, r is the number of principal components retained, $\alpha = 0.01$ represents the confidence interval, and F is the value from the F-distribution with the specified degrees of freedom [39]. Finally, the testing data is normalized by the mean and standard deviation of the training dataset, and T^2 values for the testing samples are calculated using the eigenvalue matrix generated from the training samples.

Fig. 6a shows the resulting trajectory for T^2 values for the entire run-to-failure experiment. The first point at which the T^2 values crosses the T^2 statistical limit is around 2972 operation hours, in which operation hours are the total hours that the linear positioning system has been operated from its healthy initial state. It is expected that the continuous operation of the experimental ball screw without lubrication will decrease the manufacturer-set preload as the system loses its rigidity. Fig. 6a shows that throughout the initial degradation of the ball screw, the preload loss trend is increasing. Eventually, preload is expected to be essentially nonexistent in the system, at which point the preload loss remains nearly constant. This appears to occur around 6000 h.

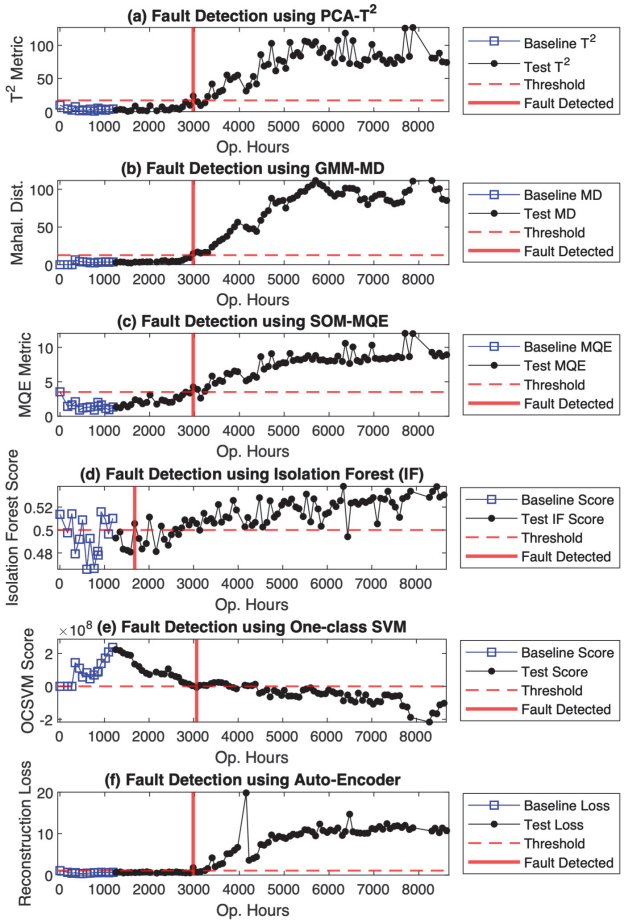

Fig. 6. Fault Detection using (a) PCA-T2, (b) GMM-MD, (c) SOM-MQE, (d) Isolation Forest, (e) One-class SVM, and (f) Auto-Encoder.

To compare the performance of the proposed methodology, five other state-of-the-art techniques [40] are implemented and explained below:

(i) Gaussian Mixture Model – Mahalanobis Distance (GMM-MD) [41]: Mixture models, especially the Gaussian Mixture Model (GMM), are widely used statistical methods. GMM is an effective universal approximator and finds use in several applications such as density estimation, clustering, association rules, outlier detection, etc. The Expectation-Maximization algorithm is used to maximize the log likelihood and estimate the mean and covariance matrix of the distribution. The principal components extracted in the PCA-T^2 approach are used in this method to reduce the dimensionality of the data and ensure successful training. The PCs of the first 15 samples are used for estimating the parameters of the model assuming the number of clusters as 1, and the PCs of the remaining samples are used for testing. Mahalanobis Distance (MD) is used as the deviation metric to identify novelty for each test point. Since MD obtained from one Gaussian component follows a β distribution [42], a β statistical limit at $\alpha = 0.01$ is used as a threshold. A moving window average with a sample width of 4 is implemented for robustness. MD values below the threshold are considered normal, while those above the threshold indicate an anomaly.

(ii) Self-Organizing Maps (SOMs) [40]: The SOM is a grid-like neural network that is largely used as an unsupervised approach for discovering clusters in a dataset and, in effect, adjusts the location of nodes in the feature space to reflect these detected clusters. The same set of baseline and test features are used in this method as the PCA-T^2 approach. The baseline features are used to train the SOM to create a kernel-based representation of normalcy. The test features are then utilized to identify novelty. The Euclidean distance between a test point and the SOM nodes, called the Minimum Quantization Error (MQE), is measured and used to determine uniqueness. A three-sigma limit on the baseline MQE values is used as a threshold for fault detection.

TABLE III
SUMMARY OF FAULT DETECTION APPROACHES & RESULTS

Method	Input	Fault Detection Metric	Detection Pt.
PCA	Selected Features	T^2	2972 hr.
GMM	PCs from PCA	MD	2972 hr.
SOM	Selected Features	MQE	2972 hr.
IF	Selected Features	Anomaly Score	1678* hr.
OCSVM	Selected Features	Anomaly Score	3069 hr.
AE	Torque. Data	Reconstruction Loss	2972 hr.

(iii) Isolation Forest (IF): An Isolation Forest [43] detects novelties by isolating them from normal points using an ensemble of isolation trees. Each isolation tree is trained for a subset of training observations, which are the baseline features here, by randomly selecting a split variable and split location until each observation in the subset falls in its own leaf node. Because anomalies are rare and unique, they settle at a distinct leaf node closer to the root node and have a shorter route length. The anomaly score of a test feature is calculated by normalizing its average path length over all isolation trees. A threshold of 0.5 [43] is used to detect novelty, where scores below 0.5 are considered normal, and above 0.5 indicate an anomaly.

(iv) One-class Support Vector Machines (SVMs): An unsupervised SVM [40] tries to separate novel data from normal data in the transformed high-dimensional predictor space. The SVM model with a linear kernel is trained using the baseline features and a class label of one. The anomaly scores are calculated for the test features with a detection threshold of zero; a positive score for a class indicates that the observation is predicted to be in the training class, and a negative score indicates otherwise. A moving window average with a sample width of 4 is implemented for robustness.

(v) Auto-encoder [44]: An autoencoder (AE) is a form of an artificial neural network that uses dimensionality reduction to learn efficient features of unlabeled inputs. By attempting to recreate the input from the encoding, the features are validated and enhanced. Unlike all methods implemented before, which use the same set of extracted features for performance comparison, the auto-encoder is implemented to compare the performance of the entire Phase I methodology and does its own automated feature extraction. To build the model, preprocessed torque signals of equal length that include both steady-state and transient portions are used. The number of baseline samples is kept the same as for other methods, and the number of hidden units is set to ten. The mean squared error between the input signal and the reconstructed signal, also called the reconstruction loss, is used as the novelty indicator. A three-sigma limit on the reconstruction loss for the baseline samples is used as a threshold for fault detection.

Fig. 6(b-f) shows that GMM-MD, SOM-MQE, and AE result in a fault detection point at 2972 hours, which is the same as the proposed PCA-T^2, while Isolation Forest detects a fault at 1678 hours and OCSVM detects a fault at 3069 hours. While the algorithm that detects the fault the earliest should be chosen, the unstable behavior of the baseline IF scores around the threshold in Fig. 6d show the untrustworthiness in the detection point. All other methods show effective training by having stable baseline scores and amplitudes showing a significant deviation towards the end of the operating life of the ball screw. A summary of the results of the fault detection approaches is presented in Table III. The similarity of the resulting detection points from these methods with the proposed PCA-T^2 indicate the validity of the selected features and the point of fault occurrence. In comparison to the implemented methods, PCA-T^2 is preferred for simplicity and practicality of use. In applications, once an occurrence of an incipient fault is indicated by the proposed method, an IMU can be used to measure the absolute errors in the ball screw as described in the next section. The error values can aid in evaluating the performance accuracy against the acceptable tolerances to plan for maintenance or replacement.

V. Phase II – Absolute Error Estimation

Signals from the IMU can be used to verify the presence of backlash and measure its magnitude. Backlash in the linear axis would create a positional shift between the positive- and negative-direction IMU signals. The proposed method will estimate the absolute error caused by backlash.

The proposed method is based on signal correlations to determine positional shifts of the six-degree-of-freedom error motions. During a reversal motion of the carriage, backlash between the ball nut and the ball screw will cause the ball screw to rotate slightly without the carriage moving. Once the carriage begins to move, the trucks will move along the same path on the rails as with no backlash, but the actual rotational position of the ball screw will now be slightly changed by a constant offset from the backlash. This slight offset causes the sensed error motions at each position to be slightly shifted at a micrometer-level. Each of the six error motion signals can be tested with correlation analysis for this slight shift. In theory, the same backlash could be estimated from any of the six signals, but in practice, due in part to different mechanical sensitivities of the errors to the ball nut and ball screw assembly, each error motion will yield a different backlash value. The backlash corresponding to the highest correlation value approximates the backlash for that dataset.

This new method can be explained in various steps. Since each error motion will be analyzed for signal shifts, any of the six error motions can be used for illustration. Fig. 7 shows the average slow-speed component, slow(), of the positioning error motion for positive-direction motion, E_{XX} ↑, for two different operation times, 924 h and 3723 h. The individual error motions from 90 runs of data collection were averaged to produce the data seen in Fig. 7. The operational difference of about 2000 h of near-constant back-and-forth motion of the axis may result in backlash. The slow-speed component is utilized because it yields the high-spatial-frequency component of the error motion [34] which should increase the sensitivity of backlash detection. A low spatial-frequency component is visible in Fig. 7a, which decreases the correlation of the signals. However, to focus on the highest-frequency components for correlation purposes, the slow-speed signals are high-pass-filtered and then windowed with a custom function called winfilt(). Fig. 8 shows the resulting signals from "winfilt" after (1) application of a high-pass filter based on a first-order Savitzky-Golay filter [45] with a spatial cutoff wavelength of 0.5 mm, (2) the removal of the means, and (3) application of a symmetric Hann window. Fig. 8b shows a greater correlation compared to Fig. 7b, as well as a visible, but slight, horizontal shift of one signal relative to the other. This shift is related to the backlash to be measured.

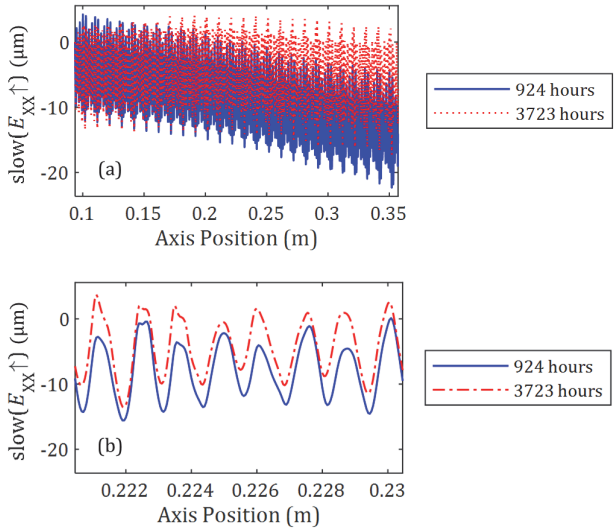

Fig. 7. (a) Slow-speed component of the positioning error motion for positive-direction motion (E_{XX} ↑) for two different operation times, and (b) zoomed-in view of the error motion component.

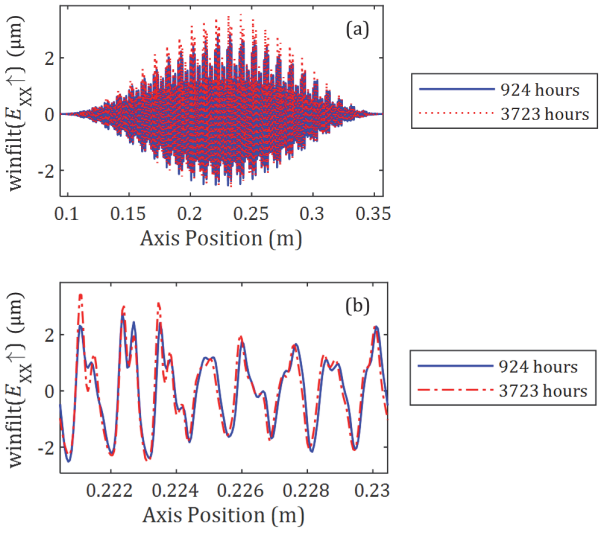

Fig. 8. (a) Windowed and filtered positioning error motion for positive-direction motion, winfilt(E_{XX} ↑), for two different operation times, and (b) zoomed-in view of winfilt(E_{XX} ↑).

Next, the correlation between the two signals is calculated as a function of a horizontal shift to estimate the overall position shift of the second signal relative to the first signal. Fig. 9a shows the correlation, corr(), of the signals in Fig. 8 as a function of axis position lag. The general shape of the

correlation is similar to the symmetric Hann window, but peaks occur when the signals are better correlated. The peaks are spaced apart by the ball screw pitch observed by the IMU, as shown in Fig. 9a. The peaks that are high enough, crossing a 75% threshold, are then fitted in a least-squares manner with polynomials for the data points with positive correlations, as seen in Fig. 9b, to determine the local position shifts. All shifts are then fitted with a least-squares line, as shown in Fig. 9c, to yield the overall position shift between the two original signals as well as the IMU-observed ball screw pitch, in this case, 1.00013 cm, which is 1.3 µm greater than the nominal ball screw pitch of 1 cm.

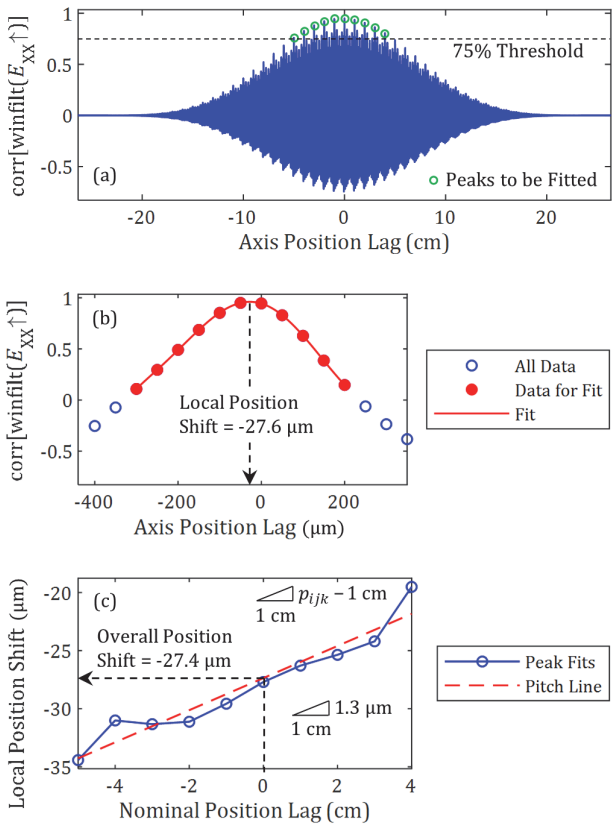

Fig. 9. (a) Correlation between windowed and filtered positioning error motion for positive-direction motion, winfilt(E_{XX} ↑), for two different operation times (924 hours and 3723 hours), (b) fit of one peak used to determine a local position shift between the signals, and (c) fitted line to all local position shifts, one for each fitted peak, to determine the overall position shift between the signals.

This correlation process to estimate the overall position shift can also be applied to negative-direction motion (e.g., E_{XX} ↓) and for any system state. The correlation value, γ_{ijk}, for any correlation process is defined as

$$\gamma_{ijk} = \max\left(\mathrm{corr}\left[\mathrm{winfilt}\left(E_{ijk}(x)\right)\right]\right) \tag{3}$$

where $E_{ijk}(x)$ is the error motion as a function of position x for the i^{th} system condition, the j^{th} error motion degree of freedom (DOF) ($j = 1, 2, \ldots 6$ for E_{XX}, E_{YX}, E_{ZX}, E_{AX}, E_{BX}, and E_{CX}, respectively), and the k^{th} axis motion direction ($k = 1$ for positive and $k = 2$ for negative). Also, an observed ball screw pitch, p_{ijk}, is associated with γ_{ijk}, as seen in Fig. 9c for the nominal ball screw pitch of 1 cm.

Fig. 10 shows the position shift between the positioning error motion (E_{XX}) at any operation time and the error motion for the initial operation time (924 h), based on the described correlation analysis. The position shifts for both positive and negative directions are typically within ±150 µm and may be as large as 2 mm, due in part to the changing origin of motion for each test. A wooden block is used as a reference to set the origin for each test, and the variability of this process causes a significant portion of the position shifts observed in Fig. 10. However, because the same origin is used for both positive and negative motion, the position shift caused by the origin-setting process is a common-mode contributor, and hence, the positive- and negative-direction curves in Fig. 10 are very similar. The recirculation of the bearing balls in the ball nut is also a contributor to the position shifts and is not inherently a common-mode contributor like the origin-setting process. Nonetheless, the positive and negative shifts are relatively close to each other, as seen in Fig. 10b. The small differences between the positive and negative position shifts will be used to determine the change in backlash.

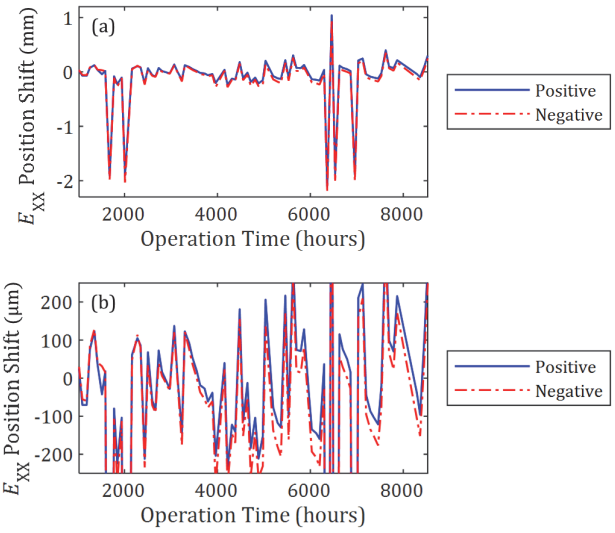

Fig. 10. (a) Position shift between the positioning error motion (E_{XX}) at any operation time and the error motion for the initial operation time (924 hours), and (b) zoomed-in view of the position shift for both motion directions.

The backlash is determined via use of the position shifts and the corresponding correlation values. First, $\mathrm{PositionShift}_{ijk}$ is defined as the position shift for the i^{th} system condition (related to operation time), j^{th} error motion DOF, and k^{th} axis motion direction. The change in position shift, $\Delta\mathrm{PositionShift}_{ij}$, is then defined as the position shift for positive-direction motion minus the position shift for negative-direction motion; that is,

$$\begin{aligned}\Delta\mathrm{PositionShift}_{ij} = {} & \mathrm{PositionShift}_{ij1} \\ & - \mathrm{PositionShift}_{ij2}\end{aligned} \tag{4}$$

Fig. 11 shows ΔPositionShift for all system conditions, due to varying operation times, and all six error motions. Most of the curves in Fig. 11 are highly correlated because all sensor

data, and hence all error motions, are correlated in time and thus position. In fact, almost all the error motions trend upwards to have changes in position of about 50 µm around 8000 operation hours. Any small trends in position could account for this trend in ΔPositionShift, e.g., due to the controller, preload, or even the accelerometer sensitivity used for E_{XX}. However, one physical difference between ΔPositionShift for E_{XX} and ΔPositionShift for any other error motion is that backlash affects ΔPositionShift for E_{XX} but not for the other error motions. Therefore, the change in backlash, $\Delta\text{Backlash}_{ij}$, for the i^{th} system condition and j^{th} error motion is defined as the difference between ΔPositionShift for E_{XX} and ΔPositionShift for the j^{th} error motion; that is,

$$\Delta\text{Backlash}_{ij} = \Delta\text{PositionShift}_{i1} - \Delta\text{PositionShift}_{ij} \tag{5}$$

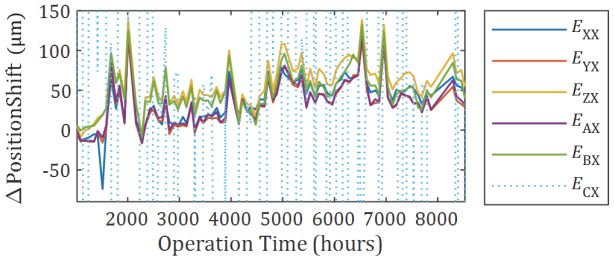

Fig. 11. Difference between the positive- and negative-direction position shifts.

For the i^{th} system condition, there are five values for $\Delta\text{Backlash}_{ij}$, one for each of the five non-positioning error motions. The estimated change in backlash for the i^{th} system condition, $\Delta\text{Backlash}_i$, is defined as a weighted sum of the individual backlash changes; that is,

$$\Delta\text{Backlash}_i = \sum_{j=2}^{6} {\gamma_{ij}}^{\sigma}\,\Delta\text{Backlash}_{ij} \Big/ \sum_{j=2}^{6} {\gamma_{ij}}^{\sigma} \tag{6}$$

where σ is a non-negative integer for weighting, and

$$\gamma_{ij} = \min\left(\gamma_{ij1}, \gamma_{ij2}\right) \tag{7}$$

Henceforth, σ is set to equal 4, so that backlash changes associated with low correlation values are penalized in Eq. (6). Also, because $\Delta\text{Backlash}_{ij}$ comes from the subtraction of two position shifts, one correlation value (γ_{ij1}) is associated with positive motion and the other correlation value (γ_{ij2}) is associated with negative motion, so Eq. (7) defines γ_{ij} conservatively as the minimum of the two associated correlations used to create that backlash.

Fig. 12 shows application of Eqs. (5)-(7). For every operation time, the horizontal straightness error motion, E_{YX}, yields the maximum correlation used for $\Delta\text{Backlash}_i$, as seen in Fig. 12a-b. Thus, the change in backlash is determined, as seen in Fig. 12c, mainly by use of E_{XX} and E_{YX} in which $\Delta\text{Backlash}_i$ is most similar to $\Delta\text{Backlash}_{i2}$ (for E_{YX}, as seen in Fig. 12b). Fig. 12 reveals that the main sensors for backlash detection are two accelerometers: the X-axis accelerometer, associated with the positioning error motion, E_{XX}, and the Y-axis accelerometer, associated with the horizontal straightness error motion, E_{YX}. The four other sensors are also utilized for backlash detection, and while they are not as significant for the given system, are still potentially very useful for other linear positioning systems.

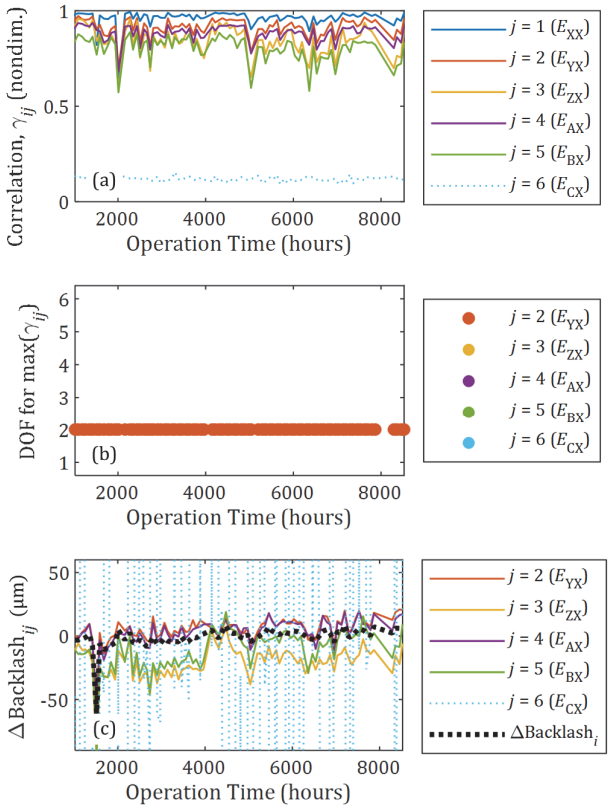

Fig. 12. (a) Correlation for each DOF, (b) the DOF corresponding to the maximum correlation, excluding the positioning error motion (E_{XX}), and (c) the individual changes in backlash and their weighted sum, the estimated change in backlash.

Fig. 13a shows the estimated change in backlash, according to Eq. (6), as a function of operation time. Experimental values and a filtered version of the estimated change in backlash, based on a Savitzky-Golay filter, are also shown. Fig. 13a reveals that the change in backlash is essentially nonexistent (0 µm) until around 2500 h of operation. As seen in Fig. 13a, a fault may have occurred around 2500 hours of operation, perhaps related to the relatively low correlation values at those times (see Fig. 12a). The backlash appears to trend upward with time thereafter.

Another approach to estimate the change in backlash is to use the change in the IMU-observed ball screw pitch (see "pitch line" in Fig. 9c). An estimated ball screw pitch, p_{ijk}, and correlation value, γ_{ijk}, exists for the i^{th} system condition, j^{th} error motion DOF, and k^{th} axis motion direction. The perceived ball screw pitch, p_i, for the i^{th} system condition is then defined as a weighted sum of the individual IMU-observed ball screw pitches; that is,

$$p_i = \sum_{j,k} ({\gamma_{ijk}}^{\sigma}) p_{ijk} \Big/ \sum_{j,k} ({\gamma_{ijk}}^{\sigma}) \tag{8}$$

where σ is the same non-negative integer for weighting as in Eq. (6). Finally, the change in backlash for the i^{th} system condition is approximately defined as

$$\Delta\text{Backlash}_i \approx \frac{L}{p}(p_i - p_0) \tag{9}$$

where L is the total travel length ($L = 0.45$ m), p is the nominal ball screw pitch ($p = 1$ cm), and p_0 is the initial operational ball screw pitch. The presence of backlash decreases the nominal travel distance from L to L minus the backlash, while the ball screw pitch remains nominally unchanged. However, because the IMU-based analysis outputs a total travel distance of L even in the presence of backlash, this process yields a perceived increase in the ball screw pitch (e.g., see Fig. 9c). Equation (9) uses the perceived ball screw pitch to essentially adjust the IMU-based travel distance to account for backlash.

Fig. 13b shows the estimated change in backlash, according to Eq. (9), as a function of operation time. The estimated change in backlash based on ball screw pitch (see Fig. 13b) is similar to the estimated change in backlash based on signal position shifts (see Fig. 13a). The filtered estimates in Fig. 13a and Fig. 13b are nominally monotonic with a significant change in backlash around 4000 h of operation and a backlash change of about 10 µm at 8000 operation hours. The backlash estimates are not identical, and both have significant high-frequency variations, yet the filtered estimates are similar in magnitude and trends. The backlash estimates based on ball screw pitch (see Fig. 13b) are generally closer to the experimental values but have significant high-frequency variations with unrealistic negative backlash changes. Hence, the backlash estimates based on signal shifts (see Fig. 13a) are more plausible with generally positive values.

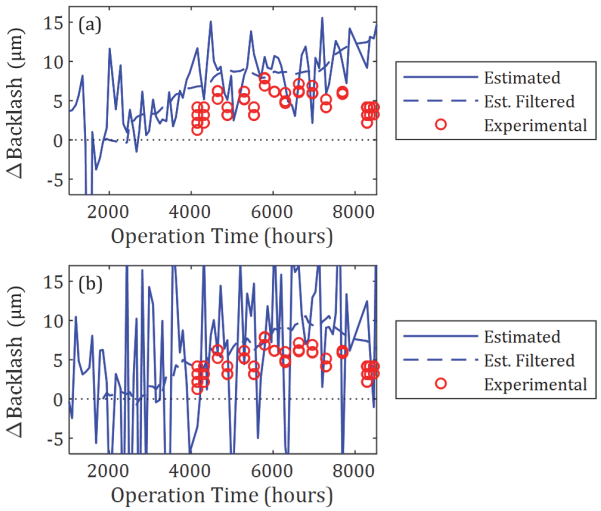

Fig. 13. Estimated backlash based on (a) signal position shifts or (b) perceived ball screw pitch, a filtered version of the estimated backlash, and experimentally measured backlash values as a function of operation time.

VI. Conclusion

The proposed two-phase approach offers a practical method for incipient fault detection and backlash quantification. In the first phase, online data streams are used to monitor for an initial fault. While the PCA-T^2 method is recommended for its simplicity, multiple health monitoring algorithms give consistent results, confirming the strength of the underlying feature extraction and selection methods.

The method developed for the second phase shows that changes in backlash may be detectable with IMU data. The high-spatial-frequency components of error motions are processed to yield a change of backlash by correlating the positioning error motion, E_{XX}, with itself, a straightness error motion (E_{YX} or E_{ZX}), or an angular error motion (E_{AX}, E_{BX}, or E_{CX}). Correlation-based estimates for the change of backlash show significant backlash changes of about 10 µm at 8000 operation hours. Thus, the IMU-based error motions are useful for estimating backlash.

Future work includes repeating the run-to-failure experiments to verify the results presented in this paper, including the general applicability of the selected fault detection and backlash monitoring feature sets. In addition, a more robust physical backlash measurement should be collected throughout the duration of the test to validate the values produced in the second phase of health monitoring.

Acknowledgement

The authors would like to express appreciation for the support from the following financial assistance award: 60NANB21D114 from the U.S. Department of Commerce, National Institute of Standards and Technology.

References

[1] J. Fleischer, A. Broos, M. Schopp, J. Wieser, and H. Hennrich, "Lifecycle-oriented component selection for machine tools based on multibody simulation and component life prediction," *CIRP Journal of Manufacturing Science and Technology,* vol. 1, no. 3, pp. 179-184, 2009, doi: https://doi.org/10.1016/j.cirpj.2008.10.006.

[2] W. H. Klein, "Zustandsüberwachung von rollen-profilschienenführungen und kugelgewindetrieben," *Apprimus Verlag,* 2011.

[3] W. Jin, Y. Chen, and J. Lee, "Methodology for ball screw component health assessment and failure analysis," presented at the ASME 2013 International Manufacturing Science and Engineering Conference, 2013, MSEC2013-1252, doi: https://doi.org/10.1115/MSEC2013-1252.

[4] C. C. Wei, J. F. Lin, and J.-H. Horng, "Analysis of a ball screw with a preload and lubrication," *Tribology International,* vol. 42, no. 11, pp. 1816-1831, 2009, doi: https://doi.org/10.1016/j.triboint.2008.12.013.

[5] P. C. Tsai, C. C. Cheng, and Y. C. Hwang, "Ball screw preload loss detection using ball pass frequency," *Mechanical Systems and Signal Processing,* vol. 48, no. 1, pp. 77-91, 2014, doi: https://doi.org/10.1016/j.ymssp.2014.02.017.

[6] P. Li *et al.*, "Prognosability study of ball screw degradation using systematic methodology," *Mechanical Systems and Signal Processing,* vol. 109, pp. 45-57, 2018, doi: https://doi.org/10.1016/j.ymssp.2018.02.046.

[7] T. L. Nguyen, S.-K. Ro, and J.-K. Park, "Study of ball screw system preload monitoring during operation based on the motor current and screw-nut vibration," *Mechanical Systems and Signal Processing,* vol. 131, pp. 18-32, 2019, doi: https://doi.org/10.1016/j.ymssp.2019.05.036.

[8] C.-G. Zhou, S.-H. Ren, H.-T. Feng, J.-W. Shen, Y.-S. Zhang, and Z.-T. Chen, "A new model for the preload degradation of linear rolling guide," *Wear,* vol. 482-483, p. 203963, 2021, doi: https://doi.org/10.1016/j.wear.2021.203963.

[9] *ISO 230-2 - test code for machine tools − part 2: Determination of accuracy and repeatability of positioning of numerically controlled axes*, International Organization for Standardization (ISO), 2014.

[10] T. L. Nguyen, Seung-Kook Ro, Chang Kyu Song, and Jong-Kweon Park, "Study on preload monitoring of ball screw feed drive system using natural frequency detection," *Journal of the Korean Society for Precision Engineering,* vol. 35, no. 2, pp. 135-143, 2018, doi: https://doi.org/10.7736/KSPE.2018.35.2.135.

[11] T. Xi, S. Kehne, T. Fujita, A. Epple, and C. Brecher, "Condition monitoring of ball-screw drives based on frequency shift," *IEEE/ASME Transactions on Mechatronics,* vol. 25, no. 3, pp. 1211-1219, 2020, doi: https://doi.org/10.1109/TMECH.2020.2969846.

[12] G.-H. Feng and Y.-L. Pan, "Investigation of ball screw preload variation based on dynamic modeling of a preload adjustable feed-drive system and spectrum analysis of ball-nuts sensed vibration signals," *International Journal of Machine Tools and Manufacture,* vol. 52, no. 1, pp. 85-96, 2012, doi: https://doi.org/10.1016/j.ijmachtools.2011.09.008.

[13] M. Benker, S. Junker, J. Ellinger, T. Semm, and M. F. Zaeh, "Experimental derivation of a condition monitoring test cycle for machine tool feed drives," *Production Engineering,* vol. 16, no. 1, pp. 55-64, 2022, doi: https://doi.org/10.1007/s11740-021-01085-9.

[14] X.-Y. Wang, H.-T. Feng, C.-G. Zhou, Z.-T. Chen, and J.-L. Xie, "A new two-stage degradation model for the preload of linear motion ball guide considering machining errors," *Journal of Tribology,* vol. 144, no. 5, 2022, doi: https://doi.org/10.1115/1.4053625.

[15] H.-X. Zhou, C.-G. Zhou, H.-T. Feng, and Y. Ou, "Theoretical and experimental analysis of the preload degradation of double-nut ball screws," *Precision Engineering,* vol. 65, pp. 72-90, 2020, doi: https://doi.org/10.1016/j.precisioneng.2020.04.012.

[16] G.-H. Feng and Y.-L. Pan, "Establishing a cost-effective sensing system and signal processing method to diagnose preload levels of ball screws," *Mechanical Systems and Signal Processing,* vol. 28, pp. 78-88, 2012, doi: https://doi.org/10.1016/j.ymssp.2011.10.004.

[17] Y.-C. Huang, C.-H. Kao, and S.-J. Chen, "Diagnosis of the hollow ball screw preload classification using machine learning," *Applied Sciences,* vol. 8, no. 7, p. 1072, 2018, doi: https://doi.org/10.3390/app8071072.

[18] B. Denkena, B. Bergmann, and A. Schmidt, "Preload monitoring of single nut ball screws based on sensor fusion," *CIRP Journal of Manufacturing Science and Technology,* vol. 33, pp. 63-70, 2021, doi: https://doi.org/10.1016/j.cirpj.2021.02.006.

[19] V. Pandhare, X. Li, M. Miller, X. Jia, and J. Lee, "Intelligent diagnostics for ball screw fault through indirect sensing using deep domain adaptation," *IEEE Transactions on Instrumentation and Measurement,* vol. 70, pp. 1-11, 2020, doi: https://doi.org/10.1109/TIM.2020.3043512.

[20] K. Chen, Zu, L. and Wang, L., "Prediction of preload attenuation of ball screw based on support vector machine," *Advances in Mechanical Engineering,* vol. 10, no. 9, pp. 1-10, 2018, doi: https://doi.org/10.1177/1687814018799161.

[21] A. Oyanguren, Larranaga, J. and Ulacia, I., "Thermo-mechanical modelling of ball screw preload force variation in different working conditions," *The International Journal of Advanced Manufacturing Technology,* vol. 97, no. 1-4, pp. 723-739, 2018, doi: https://doi.org/10.1007/s00170-018-2008-8.

[22] W.-C. Shih, F. Furqanuddin, P.-L. Lee, and J.-P. Hung, "Monitoring of preload variation of linear guide positioning stage using artificial neural network," *Applied Sciences,* vol. 11, no. 17, p. 7902, 2021, doi: https://doi.org/10.3390/app11177902.

[23] M. Benker and M. F. Zaeh, "Condition monitoring of ball screw feed drives using convolutional neural networks," *CIRP Annals,* vol. 71, no. 1, in press, 2022, doi: https://doi.org/10.1016/j.cirp.2022.03.017.

[24] M. Azamfar, X. Li, and J. Lee, "Intelligent ball screw fault diagnosis using a deep domain adaptation methodology," *Mechanism and Machine Theory,* vol. 151, p. 103932, 2020, doi: https://doi.org/10.1016/j.mechmachtheory.2020.103932.

[25] X. Li, W. Zhang, H. Ma, Z. Luo, and X. Li, "Deep learning-based adversarial multi-classifier optimization for cross-domain machinery fault diagnostics," *Journal of Manufacturing Systems,* vol. 55, pp. 334-347, 2020, doi: https://doi.org/10.1016/j.jmsy.2020.04.017.

[26] H. Shao, M. Xia, G. Han, Y. Zhang, and J. Wan, "Intelligent fault diagnosis of rotor-bearing system under varying working conditions with modified transfer convolutional neural network and thermal images," *IEEE Transactions on Industrial Informatics,* vol. 17, no. 5, pp. 3488-3496, 2021, doi: https://doi.org/10.1109/TII.2020.3005965.

[27] X. Zhao *et al.*, "Intelligent fault diagnosis of gearbox under variable working conditions with adaptive intraclass and interclass convolutional neural network," *IEEE Transactions on Neural Networks and Learning Systems,* pp. 1-15, 2022, doi: https://doi.org/10.1109/TNNLS.2021.3135877.

[28] M. Zhao, S. Zhong, X. Fu, B. Tang, S. Dong, and M. Pecht, "Deep residual networks with adaptively parametric rectifier linear units for fault diagnosis," *IEEE Transactions on Industrial Electronics,* vol. 68, no. 3, pp. 2587-2597, 2021, doi: https://doi.org/10.1109/TIE.2020.2972458.

[29] X. Zhao, J. Yao, W. Deng, M. Jia, and Z. Liu, "Normalized conditional variational auto-encoder with adaptive focal loss for imbalanced fault diagnosis of bearing-rotor system," *Mechanical Systems and Signal Processing,* vol. 170, p. 108826, 2022, doi: https://doi.org/10.1016/j.ymssp.2022.108826.

[30] X. Zhao, M. Jia, and Z. Liu, "Semisupervised graph convolution deep belief network for fault diagnosis of electormechanical system with limited labeled data," *IEEE Transactions on Industrial Informatics,* vol. 17, no. 8, pp. 5450-5460, 2021, doi: https://doi.org/10.1109/TII.2020.3034189.

[31] *ISO 230-1 - test code for machine tools − part 1: Geometric accuracy of machines operating under no-load or quasi-static conditions*, International Organization for Standardization (ISO), 2012.

[32] H. Yang *et al.*, "Remaining useful life prediction of ball screw using precision indicator," *IEEE Transactions on Instrumentation and Measurement,* vol. 70, pp. 1-9, 2021, doi: https://doi.org/10.1109/TIM.2021.3087803.

[33] H. Yang, X. Mei, G. Jiang, T. Tao, Z. Sun, and F. Zhao, "Remaining useful life prediction of ball screw under time-varying conditions with limited data," *IEEE/ASME Transactions on Mechatronics,* pp. 1-10, 2022, doi: https://doi.org/10.1109/TMECH.2022.3144351.

[34] G. W. Vogl, M. A. Donmez, and A. Archenti, "Diagnostics for geometric performance of machine tool linear axes," *CIRP Annals-Manufacturing Technology,* vol. 65, no. 1, pp. 377-380, 2016, doi: https://doi.org/10.1016/j.cirp.2016.04.117.

[35] G. W. Vogl, N. J. Jameson, A. Archenti, K. Szipka, and M. A. Donmez, "Root-cause analysis of wear-induced error motion changes of machine tool linear axes," *International Journal of Machine Tools and Manufacture,* vol. 143, pp. 38-48, 2019, doi: https://doi.org/10.1016/j.ijmachtools.2019.05.004.

[36] R. A. Fisher, "The use of multiple measurements in taxonomic problems," *Annals of Eugenics,* vol. 7, no. 2, pp. 179-188, 1936, doi: https://doi.org/10.1111/j.1469-1809.1936.tb02137.x.

[37] H. Hotelling, "Analysis of a complex of statistical variables into principal components," *Journal of Educational Psychology,* vol. 24, no. 6, pp. 417-441, 1933, doi: https://doi.org/10.1037/h0071325.

[38] L. Mujica, J. Rodellar, A. Fernández, and A. Güemes, "Q-statistic and T2-statistic PCA-based measures for damage assessment in structures," *Structural Health Monitoring,* vol. 10, no. 5, pp. 539-553, 2011, doi: https://doi.org/10.1177/1475921710388972

[39] H. Hotelling, "Multivariate quality control illustrated by air testing of sample bombsights," in *Techniques of statistical analysis*, C. Eisenhart, M. W. Hastay, and W. A. Wallis Eds. New York: McGraw-Hill, 1947, pp. 111-184.

[40] M. A. F. Pimentel, D. A. Clifton, L. Clifton, and L. Tarassenko, "A review of novelty detection," *Signal Processing,* vol. 99, pp. 215-249, 2014, doi: https://doi.org/10.1016/j.sigpro.2013.12.026.

[41] V. Pandhare, X. Jia, and J. Lee, "Collaborative prognostics for machine fleets using a novel federated baseline learner," presented at the Annual Conference of the PHM Society, 2021, doi: https://doi.org/10.36001/phmconf.2021.v13i1.2989.

[42] D. Ververidis and C. Kotropoulos, "Gaussian mixture modeling by exploiting the mahalanobis distance," *IEEE Transactions on Signal Processing,* vol. 56, no. 7, pp. 2797-2811, 2008, doi: https://doi.org/10.1109/TSP.2008.917350.

[43] F. T. Liu, K. M. Ting, and Z.-H. Zhou, "Isolation-based anomaly detection," *ACM Transactions on Knowledge Discovery from Data,* vol. 6, no. 1, p. Article 3, 2012, doi: https://doi.org/10.1145/2133360.2133363.

[44] B. B. Thompson, R. J. Marks, J. J. Choi, M. A. El-Sharkawi, H. Ming-Yuh, and C. Bunje, "Implicit learning in autoencoder novelty assessment," presented at the Proceedings of the 2002 International Joint Conference on Neural Networks (IJCNN'02), Honolulu, HI, USA, 2002, doi: https://doi.org/10.1109/IJCNN.2002.1007605.

[45] A. Savitzky and M. J. E. Golay, "Smoothing and differentiation of data by simplified least squares procedures," *Analytical chemistry,* vol. 36, no. 8, pp. 1627-1639, 1964, doi: https://doi.org/10.1021/ac60214a047.

Vibhor Pandhare received his B.Tech. and M.Tech. dual degree in mechanical engineering with a specialization in production and industrial engineering from IIT Indore, India, in 2016. He received his Ph.D in mechanical engineering at the University of Cincinnati, Cincinnati, OH, USA in 2021. He was a Research Associate at IIT Mumbai, India, in 2016. His research interests include prognostics and health management, Industrial AI, Deep Learning, and Federated Learning.

Marcella Miller received the B.S. and an M.Eng. degrees in mechanical engineering from the University of Cincinnati, Cincinnati, OH, USA, in 2019, where she is currently pursuing the Ph.D. degree in mechanical engineering with the Department of Mechanical and Materials Engineering. Her research interests include prognostics and health management, machine learning, and probabilistic methods.

Gregory W. Vogl received the Bachelor's degree in Engineering Science and Mechanics and Master's degree and Ph.D. in Engineering Mechanics from Virginia Polytechnic Institute and State University of Blacksburg, Virginia, USA in 2000, 2003, and 2006, respectively. He designed, fabricated, and experimented on microelectromechanical systems as a National Research Council Postdoctoral Researcher at the National Institute of Standards and Technology (NIST). He then joined the Production Systems Group at NIST, in which he worked on standards development for machine tools and vibration metrology for accelerometers. Currently, Dr. Vogl develops sensor-based solutions for real-time health assessment of components and processes within machine tools. For his contributions, Dr. Vogl is the recipient of a NIST Engineering Laboratory Mentoring Award, NIST Colleagues' Choice Award, and NIST Engineering Laboratory Outstanding Publication Award.

Jay Lee received the B.S. degree in electrical engineering from Tamkang University, Taipei City, Taiwan, and the M.S. degree in electrical engineering from the University of Wisconsin Madison, Madison, WI, USA, and the Ph.D. degree from George Washington University, Washington, DC, USA. He is currently an Ohio Eminent Scholar, a L. W. Scott Alter Chair Professor, and a Distinguished University Professor with the University of Cincinnati, Cincinnati, OH, USA. He is the Founding Director with the National Science Foundation (NSF) Industry/University Cooperative Research Center on Intelligent Maintenance Systems, which is a multicampus NSF Industry/University Cooperative Research Center consisting of the University of Cincinnati (lead institution), the University of Michigan, Ann Arbor, MI, USA, the Missouri University of S&T, Rolla, MO, USA, and the University of Texas-Austin, Austin, TX, USA. Since its inception in 2001, the Center has been supported by more than 90 global companies and was ranked with the highest economic impacts (270:1) by NSF Economics Impacts Report in 2012.